General Disclaimer

One or more of the Following Statements may affect this Document

- This document has been reproduced from the best copy furnished by the organizational source. It is being released in the interest of making available as much information as possible.

- This document may contain data, which exceeds the sheet parameters. It was furnished in this condition by the organizational source and is the best copy available.

- This document may contain tone-on-tone or color graphs, charts and/or pictures, which have been reproduced in black and white.

- This document is paginated as submitted by the original source.

- Portions of this document are not fully legible due to the historical nature of some of the material. However, it is the best reproduction available from the original submission.

Produced by the NASA Center for Aerospace Information (CASI)

NASA Technical Memorandum 79236

DISPERSION OF SOUND IN A COMBUSTION
DUCT BY FUEL DROPLETS AND SOOT PARTICLES

J. H. Miles
Lewis Research Center
Cleveland, Ohio

and

D. D. Raftopoulos
University of Toledo
Toledo, Ohio

DISPERSION OF SOUND IN A COMBUSTION DUCT BY FUEL
DROPLETS AND SOOT PARTICLES

by Jeffrey H. Miles

National Aeronautics and Space Administration

Lewis Research Center

Cleveland, Ohio

and

D. D. Raftopoulos

The University of Toledo

Toledo, Ohio

Disperson and attenuation of acoustic plane wave disturbances pro-
pagating in a ducted combustion system are studied. The dispersion and
attenuation are caused by fuel droplet and soot emissions from a jet en-
gine combustor. The attenuation and dispersion are due to heat transfer
and mass transfer and viscous drag forces between the emissions and the
ambient gas. Theoretical calculations show sound propagation at speeds
below the isentropic speed of sound at low frequencies. Experimental re-
sults are in good agreement with the theory.

LIST OF SYMBOLS

A	matrix
A_E	soot particle exterior area per unit mass, m^2/kg
A_I	soot particle interior area per unit mass, m^2/kg
a	area, m^2
a_j, b_j	curve fit parameters
c	soot mass, kg
$c(\omega)$	sound propagation velocity, m/sec
c_o	isentropic speed of sound, m/sec
c_p	gas specific heat at constant pressure, J/kg-K
c_s	soot particle specific heat, J/kg-K
d	diameter, m

F	particle force exerted on gas
$F(\omega)$	transfer function for response of particle force on gas to pressure perturbation
f	frequency, Hz
f_R	repetition frequency, Hz
H	heat-transfer coefficient, W/m^2-K
h	enthalpy, J/kg .
i	$(-1)^{1/2}$
j	summation index (Eq. (53))
k	propagation wave number, ω/c_o, m^{-1}
k_a	effective chemical reaction rate, kg/N-sec
k_l	chemical reaction rate of the lth process
L	space between two points in duct
$H(\omega)$	transfer function for response of mass source to pressure perturbation
$(MW)_c$	molecular weight of soot
m_s	soot particle mass, kg
N	number of Fourier series curve fit parameters (Eq. (53))
Nu_H	heat-transfer Nusselt number, Hd/K
n	number of particles per unit volume
n_i, n_e	number of moles
P_o	unperturbed pressure, N/m^2
P_{o,O_2}	partial pressure of oxygen, N/m^2
p	pressure perturbation, N/m^2
Q	heat transferred to gas from particles by convection
Q_c	heat generated by chemical reaction per unit mass of fuel, J/kg
R	gas constant
r_s	radius, m
$S(\omega)$	transfer function for response of entropy source to a pressure perturbation
s	entropy of gas, J/kg-K
T	temperature, K

t	temperature perturbation, K
$\vec{U}$	system forcing function
u	velocity perturbation, m/sec
V	mean flow velocity, m/sec
$\dot{w}_{air}$	air mass flow rate, kg/sec
x	cartesian coordinate
$\vec{Y}$	system state vector
Y	relative concentration, partial pressure ratio or density ratio
y	partial pressure ratio perturbation
α	acoustic attenuation coefficient, dB/m
γ	specific heat ratio of gas
ϵ	chemical heat parameter, $Q_c/c_p T_o$
ζ	chemical reaction rate parameter, $(T_o/k_a)(dk_a/dT)$
θ	cross-spectrum phase angle
θ	time, sec
κ	gas thermal conductivity, W/m-K
$\aleph_s$	soot particle mass fraction, $n\,m_s/\rho_o$
μ	gas dynamic viscosity, kg/m-sec
ρ	gas density perturbation, kg/m^3
ρ_o	unperturbed gas density, kg/m^3
τ	Stokes relaxation time, $m/6\pi r_s \mu$, sec
τ_A	adsorption relaxation time, $1/A_I k_a P_o$, sec
τ_o	propagation time delay, sec
τ_s	soot particle thermal relaxation time, $(m_s c_p)/4\pi r_s^2 (Nu_H/d_s)\kappa$, sec
$\Phi[\ ]$	Fourier transform operator
φ	mass source rate perturbation
Ω	dispersion-attenuation propagation wave number factor
ω	angular frequency, radians/sec

Subscripts:

a	adsorbed
C	carbon
H	heat transfer
m	measured

O_2 molecular oxygen

o   reference state

R   repetition

S   soot

s   soot particle interior surface

T   total

∞   in bulk gas far from soot particle

INTRODUCTION

Pressure spectra measurements were made for a combustion noise research program in a liquid fuel ducted combustion test facility at the NASA Lewis Research Center. An examination of the measurements showed that they contained axial resonance peaks which could not be correlated using the isentropic speed of sound and the facility geometry. Consequently, the variation in the sound propagation speed which might occur when a plane wave propagates through a cloud of liquid fuel droplets or through a cloud of solid soot particles was investigated.

The literature contains a number of theoretical and experimental studies of the propagation of a plane wave through a cloud of particles. Studies considering viscous and thermal interaction but not mass transfer were made by Epstein and Carhart (Ref. 1), Chow (Ref. 2), Temkin and Dobbins (Ref. 3), and Dobbins and Temkin (Ref. 4). Studies which consider water vapor mass transfer in addition to viscous and thermal interaction were made by Marble and Wooten (Ref. 5) and were extended by Davidson (Ref. 6). The theory was confirmed experimentally by Cole and Dobbins (Ref. 7). Marble and Candel (Ref. 8) suggested that one technological application of the theory would be to use a water aersol to attenuate sound in ducts.

The significant contribution of this paper is the application of the previous work on plane waves propagating in a water aersol to the study of the possible consequences of plane waves propagating in the emissions of a liquid fuel combustor. The problem is formulated in the next section. Following this is a discussion of a calculation of attenuation and dispersion of a plane wave propagating through a liquid fuel droplet cloud. This discussion is based on the equations Marble and

Candel (Ref. 8) derived for a cloud of water droplets with just a change in droplet particle properties. Next, the propagation of a plane wave through a cloud of solid soot particles is analyzed using the approach of Marble and Candel (Ref. 8); modifications are used to account for the physics and chemistry of the soot particles. Then, sample calculations of attenuation and dispersion using assumed parameters for the propagation of a plane wave through a cloud of liquid fuel droplets and a cloud of solid soot particles are presented. This paper concludes with a discussion of the experimental results that can be compared with the theory proposed herein.

I. PROBLEM FORMULATION

A. Wave equation

Equations are presented for sound propagation through a two-phase medium consisting of a cloud of solid or liquid particles suspended in a gas. The formulation follows that of Marble and Candel (Ref. 8). The equations are based on the following assumptions:

(1) The particulate mass fraction and volume fraction are small.

(2) The particulate spacing is smaller than the acoustic wavelengths considered. Therefore, the particle cloud and gas can be treated as a continuum.

(3) The fluctuations of pressure, density, temperature, entropy, and velocity are small compared with their mean values. Therefore, the squares and cross products of these parameters can be neglected.

(4) The fluid velocity is much smaller than the speed of sound.

(5) The bulk gas can be treated as a perfect gas.

The one-dimensional, gas, linearized conservation equations for zero mean flow relating the perturbation velocity, pressure, and density (from Ref. 8) are as follows:

Continuity:

$$\frac{\partial \rho}{\partial \theta} + \frac{\rho_o \partial u}{\partial x} = \varphi \tag{1}$$

Momentum:

$$\frac{\rho_o \partial u}{\partial \theta} + \frac{\partial p}{\partial x} = F \tag{2}$$

The ideal gas entropy equation is

$$\frac{p - \rho c_o^2}{\rho_o c_o^2} = \frac{p}{\gamma P_o} - \frac{\rho}{\rho_o} = \frac{s}{c_p}$$ (3)

Marble and Candel derived from Eqs. (1) to (3) an expression for the sound propagation velocity and the sound energy attenuation for a plane wave propagating in a particle cloud. They applied the expression to a plane wave propagating in a cloud of small water droplets. The wave number equation obtained (from Ref. 8) by retaining only linear terms in small quantities for a plane pressure wave taken to be proportional to $e^{i(k\Omega x - \omega\theta)}$ is, in terms of the notation used herein and after some algebraic manipulation,

$$ik_o\Omega = i\left\{\frac{\omega}{c_o} - \frac{i}{2c_o}\left[\frac{M(\omega)}{\rho_o} - \frac{i\omega S(\omega)}{c_p} + \frac{F(\omega)}{\rho_o c_o}\right]\right\}$$ (4)

The transfer functions $M(\omega)$, $S(\omega)$, and $F(\omega)$, which relate a pressure perturbation to a perturbation in mass production, entropy production, and viscous force drag, respectively, are defined herein as

$$\Phi\left[\frac{F}{\rho_o}\right] = \frac{F(\omega)}{\rho_o c_o} \, \Phi\left[\frac{p}{\gamma P_o}\right]$$ (5)

$$\Phi\left[\frac{\varphi}{\rho_o}\right] = \frac{M(\omega)}{\rho_o} \, \Phi\left[\frac{p}{\gamma P_o}\right]$$ (6)

$$\Phi\left[\frac{s}{c_p}\right] = \frac{S(\omega)}{c_p} \, \Phi\left[\frac{p}{\gamma P_o}\right]$$ (7)

where the Fourier transform operator is

$$\Phi\left[g(\theta)\right] = \int_{-\infty}^{\infty} g(\theta)e^{+i\omega\theta} \, d\theta = G(\omega)$$ (8)

By definition, the sound propagation velocity is related to the wave number equation by

$$c(\omega) = \frac{\omega}{Im(ik_o\Omega)} \text{ m/sec}$$ (9)

Also by definition, the acoustic energy attenuation coefficient in Nepers per meter is

$$\alpha = -2 \, Re(ik\Omega)$$

Nepers per meter is converted to decibels per meter by multiplying by $10 \log_{10} e = 4.34$:

$$\alpha = -8.68 \, \text{Re}(ik_o \Omega) \tag{10}$$

B. Response of fuel droplet cloud

Fuel droplet emissions from combustors in the combustion duct system can occur when the fuel droplet spray consists of large-diameter drops and the air injected around the fuel nozzle through swirlers mixes poorly with the fuel spray. This combination of large fuel drops and poor mixing produces high levels of hydrocarbon emission (Ref. 9). The larger droplets which pass through the high temperature reaction zone are assumed to evaporate in a relatively cool gas mixture having a low oxygen concentration. Accordingly, the process is approximated herein by considering evaporation without combustion.

The processes and assumptions typically employed in an analysis of fuel drop evaporation are discussed in Refs. 10 and 11. However, rather than using a complex model to obtain expressions for (ω), (ω), and $F(\omega)$, the approximate model used in Ref. 8 for water drop evaporation was adapted for use herein by making appropriate assumptions. The resulting expressions provide (1) a guide to the order of magnitude of the transfer functions $H(\omega)$, $C(\omega)$ and $F(\omega)$ and (2) information on the frequency dependence of the sound propagation speed and attenuation. Because the resulting expressions are identical to those which could be obtained from expressions in Ref. 8, they are not shown in this paper. The numerical values of the factors in these expressions are different because the physical properties were changed to those for a fuel drop rather than those for a water drop. The results of these calculations are discussed in a later section.

C. Response of soot particle cloud

Soot produced by gas turbine combustors oxidizes as it flows through the duct system (Refs. 12 to 14). In order to calculate accurately the response of a cloud of soot particles to an acoustic pressure perturbation, the mass distribution, the chemical composition, and the distribution of particle shapes and sizes should be known. It is also necessary to know

the rate constants for the heterogeneous oxidation process and the heat-transfer process. However, at this time, none of this information is known accurately. Consequently, the following model is a simulation that includes the basic physics and chemistry in an approximate manner. An experimental study of the oxidation of soot (discussed in Ref. 15) and a mathematical model for the gasification of coal char (discussed in Ref. 16) were useful in formulating the approach used in this work. The model is based on the assumption that the soot particles can be treated as being made of porous carbon, having a spherical shape, and having a uniform temperature.

The transfer functions $H(\omega)$, $S(\omega)$, and $F(\omega)$ are derived from equations that describe the particulate phase of the one-dimensional flow of gas-soot particle mixture with interphase transfer of mass, momentum, and energy. When specifying the functional dependence of $\vdash(\omega)$ and $S(\omega)$, the following selection is made. For the force acting on the gas due to a particle, Stokes' viscous drag law is used. Thus, the total force on the gas is

$$F = -n6\pi r_s \mu(u - u_s) \tag{11}$$

For the heat transfer from the particles to the gas, Newton's law of convection is used. Thus, the total heat transfer from n soot particles into a unit volume of gas having thermal conductivity K is

$$Q = n\left(4\pi r_s^2\right)\left(\frac{Nu_H}{d_s}\right) K(t_s - t_\infty) \tag{12}$$

where Nu_H equals 2 if the air is stagnant. This value of 2, which is generally used, is used herein since the difference between the particle velocity and the gas velocity is assumed small. The general assumptions associated with using these equations are well known (Ref. 3).

The viscous drag transfer function is discussed first. A soot particle of mass m_s and radius r_s is moving at velocity u_s in the gas. The gas has a velocity u due to the wave motion. The particle experiences a Stokes drag force of $6\pi r_s \mu(u - u_s)$, and the resulting particle equation of motion is

$$m \frac{du_s}{d\theta} = 6\pi r_s \mu (u - u_s) \tag{13}$$

The gas velocity is related to a pressure perturbation for small perturbations by

$$u = c_o \frac{p}{\gamma P_o} \tag{14}$$

The Fourier transform of Eq. (13) yields the following expression for the response of the particle velocity to a pressure perturbation:

$$u_s = \frac{1}{1 + (-i\omega)\tau} c_o \left(\frac{p}{\gamma P_o}\right) \tag{15}$$

where

$$\tau = \frac{m}{6\pi r_s \mu} \tag{16}$$

Physically, τ is the time interval in which the particle velocity is reduced by a factor of $1/e$ from its initial value due to the Stokes drag force. Substituting Eq. (15) into Eq. (11) and using Eq. (5) yield the following expression for the viscous drag force perturbation in response to a pressure perturbation:

$$\Phi\left[\frac{F}{\rho_o c_o}\right] = -\frac{n6\pi r_s \mu}{\rho_o c_o} \left(\frac{c_o p}{\gamma P_o}\right) \frac{(-i\omega)\tau}{1 + (-i\omega)\tau} \tag{17}$$

Consequently, the viscous drag force transfer function is given by

$$\frac{F(\omega)}{\rho_o c_o} = -\frac{\chi_s}{\tau}\left[\frac{(-i\omega)\tau}{1 + (-i\omega)\tau}\right] \tag{18}$$

where

$$\chi_s = \frac{nm}{\rho_o} \tag{19}$$

The heat generated by the oxidation of a soot particle is assumed to be transferred directly to the particle. Thus, the entropy source term may be calculated considering only the heat transfer between the n particles and the bulk gas using Eq. (12) as follows:

$$T_o \rho_o \frac{ds}{d\theta} = Q = n\left(4\pi r_s^2\right)\left(\frac{Nu_H}{d_s}\right) K(t_s - t_\infty) \tag{20}$$

The differential equation for the entropy source can then be written as

$$\frac{d}{d\theta}\left(\frac{s}{c_p}\right) = \frac{\mathcal{R}_s}{\tau_s}\left(\frac{t_s - t_\infty}{T_0}\right) \tag{21}$$
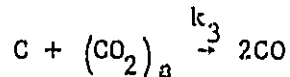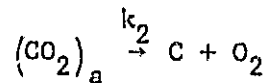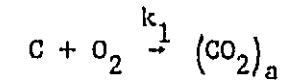
where

$$\tau_s = \frac{m_s c_p}{4\pi r_s^2 \left(\frac{Nu_H}{d_s}\right)\kappa} \tag{22}$$

Physically, τ_s is the time interval in which the gas entropy is changed by a factor of $1/e$ from it initial value.

Perturbations in bulk gas temperature and pressure are related to perturbations in soot particle temperature by taking the derivative of the bulk gas energy equation (Eq. (3)) and using the perfect gas law and Eq. (21) to show

$$\frac{d}{d\theta}\left(\frac{t_\infty}{T_0}\right) - (\gamma - 1)\frac{d}{d\theta}\left(\frac{p}{\gamma P_0}\right) = \frac{\mathcal{R}_s}{\tau_s}\left(\frac{t_s - t_\infty}{T_0}\right) \tag{23}$$

The slowest process in the burning of a soot particle controls the reaction rate. Depending on the temperature and the particle geometry, this may either be the diffusion of oxygen to the particle surface or the chemical reaction rate at the surface. For the model discussed herein, the chemical reaction rate is assumed to be slower then the diffusion rate. Consequently, it controls the oxidation process. The soot is, for simplicity, assumed to be carbon. However, evidence exists that the soot contains a few percent hydrogen which, in practice, could be important. To model the chemical reaction of oxygen with the soot, an adsorption/ desorption mechanism is used involving the following sequence of reactions:

$$C + O_2 \xrightarrow{k_1} (CO_2)_a$$

$$(CO_2)_a \xrightarrow{k_2} C + O_2$$

$$C + (CO_2)_a \xrightarrow{k_3} 2CO$$

where $(CO_2)_a$ is surface oxide (i.e., an O_2 molecule adsorbed on the carbon surface (Refs. 15 and 16)). This process may be followed by a gasification reaction which produces carbon dioxide (Ref. 15). Only the initial production of carbon monoxide is considered herein.

The following concentration equations can be written for the sequence of chemical reactions considered:

$$\frac{d}{d\theta}\left[\left(CO_2\right)_a\right] = k_1[O_2] - k_2\left[\left(CO_2\right)_a\right] - k_3\left[\left(CO_2\right)_a\right] \tag{24}$$

$$-\frac{d[c]}{d\theta} = -k_2\left[\left(CO_2\right)_a\right] + k_1[O_2] \tag{25}$$

The concentration of $\left(CO_2\right)_a$ is assumed constant because a steady-state condition is achieved where as much is created as is destroyed. Consequently, the time derivative of $\left(CO_2\right)_a$ is zero. Thus, the left side of Eq. (24) can be set to zero, and the following expression for the concentration of $\left(CO_2\right)_a$ is obtained:

$$\left[\left(CO_2\right)_a\right] = \frac{k_1[O_2]}{k_2 + k_3} \tag{26}$$

The carbon consumption rate, which equals the net rate at which mass is added to the gas by a single particle per unit particle surface area, is then given by

$$\frac{d[c]}{d\theta} = k_1[O_2] - \frac{k_2 k_1[O_2]}{k_2 + k_3} = \frac{k_1 k_3}{k_2 + k_3}\frac{P_{o,O_2}}{RT} = k_a P_{o,O_2} \tag{27}$$

The following Arrhenius model chemical reaction rates (from Ref. 16) were determined empirically to fit a wide range of data:

$$k_3 = 9500\ e^{-19,700/T}\quad kg/m^2\text{-sec} \tag{28}$$

$$\frac{k_1}{RT} = 2\times10^{-2}\ e^{-15,700/T}\quad kg/N\text{-sec} \tag{29}$$

$$k_2 = 5.5\times10^7\ e^{-38,700/T}\quad kg/m^2\text{-sec} \tag{30}$$

The rate of mass addition to the bulk gas per unit volume for soot particles having surface area a is then

$$\varphi_T = n a k_a P_{O_2} \tag{31}$$

For a small perturbation in surface temperature and oxygen partial pressure, the resulting change in mass addition can be written as

$$\varphi_T = \varphi_o + \varphi = nak_a \left(1 + \frac{T_o}{k_a} \frac{dk_a}{dT} \frac{t_s}{T_o}\right) P_{o,O_2} \left(1 + \frac{P_{O_2}}{P_{o,O_2}}\right) \qquad (32)$$

Thus, the mass perturbation term is given by

$$\varphi = (nak_a P_o) \left(\frac{P_{o,O_2}}{P_o}\right) \left[\left(\frac{T_o}{k_a} \frac{dk_a}{dT}\right) \frac{t_s}{T_o} + \frac{P_{O_2}}{P_{o,O_2}}\right] \qquad (33)$$

This equation is rewritten as

$$\frac{\varphi}{P_o} = \frac{A_s}{\tau_a} Y_{O_2} \zeta \frac{t_s}{T_o} + \frac{A_s}{\tau_a} Y_{O_2} \frac{P_{O_2}}{P_{o,O_2}} \qquad (34)$$

where

$$\tau_a = \frac{1}{A_I k_a P_o} \qquad (35)$$

$$A_I = \frac{a_s}{m_s} \qquad (36)$$

$$Y_{O_2} = \frac{P_{o,O_2}}{P_o} \qquad (37)$$

and

$$\zeta = \frac{T_o}{k_a} \frac{dk_a}{dT} \qquad (38)$$

The external surface area of a spherical carbon particle of diameter d per unit mass is

$$A_E = \frac{4\pi r_s^2}{m_s} = \frac{4\pi r_s^3}{\frac{4}{3}\pi r_s^3} \frac{1}{2000} \frac{m^2}{kg} = \frac{3}{2000d} \frac{m^2}{kg} \qquad (39)$$

Typical internal surface areas per unit mass of coal char as measured by molecular adsorption are 100,000 to 400,000 m^2/kg for 100μ particles which is four orders of magnitude greater than the external surface area per unit mass (Ref. 16). Consequently, the model calculations made herein use internal surface areas per unit mass approximately four orders of magnitude greater than the external surface areas per unit mass. The oxidation reaction is

$$C + \frac{1}{2} O_2 \rightarrow CO$$
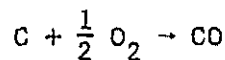
The heat generated is given by

$$Q_c = \left(\sum_P n_i h_i - \sum_R n_e h_e \right) \frac{1}{(MW)_c} \qquad (40)$$

The heat balance equation for a soot particle is then

$$\frac{d}{d\theta} (m_s c_s t_s) = -\left(4\pi r_s^2\right)\left(\frac{Nu_H}{d_s}\right) \kappa (t_s - t_\infty) - Q_c \frac{\varphi}{n} \qquad (41)$$

When all n particles are considered, Eq. (41) becomes

$$\kappa_s \frac{c_s}{c_p} \frac{d}{d\theta}\left(\frac{t_s}{T_o}\right) = -\frac{\kappa_s}{\tau_s}\left(\frac{t_s - t_\infty}{T_o}\right) - \epsilon \frac{\varphi}{P_a} \qquad (42)$$

where

$$\epsilon = \frac{Q_c}{T_o c_p} \qquad (43)$$

The perturbation in the partial pressure of oxygen is related to the mass source variation and the total pressure perturbation using the continuity equations. The oxygen continuity equation is

$$\frac{\partial}{\partial \theta} \rho_{O_2} + \rho_{o,O_2} \frac{\partial u}{\partial x} = -\varphi \frac{16}{12} \qquad (44)$$

This is because when a mass of carbon φ is added to the gas the oxygen concentration is reduced by $\frac{16}{12}\varphi$. The bulk gas continuity equation is

$$\frac{\partial \rho}{\partial \theta} + \rho_o \frac{\partial u}{\partial x} = \varphi \qquad (45)$$

The velocity gradient is eliminated from Eqs. (44) and (45) as follows:

$$\frac{\partial u}{\partial x} = \frac{\varphi}{\rho_o} - \frac{1}{\rho_o}\frac{\partial \rho}{\partial \theta} = \frac{-\frac{16}{12}\varphi}{\rho_{o,O_2}} - \frac{1}{\rho_{o,O_2}}\frac{\partial \rho_{O_2}}{\partial \theta} \qquad (46)$$

Thus,

$$\frac{\varphi}{\rho_o}\left(1 + \frac{\rho_o}{\frac{12}{16}\rho_{o,O_2}}\right) = \frac{1}{\rho_o}\frac{\partial \rho}{\partial \theta} - \frac{1}{\rho_{o,O_2}}\frac{\partial \rho_{O_2}}{\partial \theta} \qquad (47)$$

However, the temperature of the oxygen and the bulk gas are identical, and the gas properties are assumed to be identical; that is, both behave as perfect gases. Consequently, Eq. (47) can be written in terms of pressure perturbations as follows:

$$\frac{\varphi}{\rho_0}\left(\frac{\frac{12}{16}Y_{O_2}+1}{\frac{12}{16}Y_{O_2}}\right) = \frac{i}{i\omega}\left(\frac{p}{P_0} - \frac{P_{O_2}}{P_{0,O_2}}\right) \tag{48}$$

Equation (34) and the Fourier transforms of Eqs. (23), (42), and (48) can be put in the following matrix form:

$$\vec{Y} = \begin{bmatrix} 0 & -\dfrac{\aleph_s Y_{O_2}\zeta}{\tau_a} & 1 & \dfrac{\aleph_s Y_{O_2}}{\tau_a} \\[2ex] \left(-i\omega+\dfrac{\aleph_s}{\tau_s}\right) & -\dfrac{\aleph_s}{\tau_s} & 0 & 0 \\[2ex] \dfrac{\aleph_s}{\tau_s} & \left[\dfrac{\aleph_s c_s(-i\omega)}{c_p}+\dfrac{\aleph_s}{\tau_s}\right] & \epsilon & 0 \\[2ex] 0 & 0 & \dfrac{1}{\gamma}\left[\dfrac{Y_{O_2}\frac{12}{16}+1}{Y_{O_2}\frac{12}{16}}\right] & \left(\dfrac{i\omega}{\gamma}\right) \end{bmatrix} \begin{bmatrix} \dfrac{t_\omega}{T_0} \\[2ex] \dfrac{t_s}{T_0} \\[2ex] \dfrac{\varphi}{\rho_0} \\[2ex] \dfrac{P_{O_2}}{P_{0,O_2}} \end{bmatrix} = \begin{bmatrix} 0 \\[2ex] -i\omega(\gamma-1) \\[2ex] 0 \\[2ex] (-i\omega) \end{bmatrix} \left(\dfrac{p}{\gamma P_0}\right) = \vec{U} \tag{49}$$

The solution is

$$\vec{Y} = A^{-1}\vec{U} \tag{50}$$

The mass source transfer function is found by using the solution for φ/ρ_0 obtained from Eq. (49) and Eq. (6). The entropy source transfer function is found using the quantities t_s/T_0 and t_ω/τ_ω which were obtained from Eq. (49), the Fourier transform of Eq. (21), and Eq. (7).

D. Sample calculations

A typical dispersion curve and an attenuation curve calculated for vaporizing fuel droplets by using the arbitrary parameters in Table I are presented in Fig. 1(a). The propagation velocity varies from 506 m/sec at low frequencies to the isentropic speed of sound (610 m/sec) at high frequencies. The attenuation is greater than 3 dB/m above 400 Hz. Figure 1(b) shows the relative importance of the transfer functions $M(\omega)$, (ω), and (ω). From Fig. 1(b) it follows that the viscous drag force

transfer function can be neglected below 1200 Hz. Above 1200 Hz the entropy transfer function becomes less than the viscous drag force transfer function and it is easily shown that this accounts for the increase in the attenuation.

A typical dispersion curve and an attenuation curve calculated for oxidizing soot particles by using the arbitrary parameters in Table II are shown in Fig. 2 for mass loadings of 0.0058 (example 1, Table II) and 0.00058 kg/m^3 (example 2, Table II) and an oxygen partial pressure of 0.05. The sound propagation speed varies from 440 m/sec for a mass loading of 0.00058 and from 420 m/sec for a mass loading of 0.0058 at low frequencies to the isentropic speed of sound (610 m/sec) at high frequencies. The attenuation for a mass loading of 0.0058 is greater than 3 dB/m above 400 Hz. However, it drops to less than 1 dB/m for a mass loading of 0.00058. It was also found that for these cases the viscous drag force transfer function could be neglected below 1200 Hz.

II. EXPERIMENTAL INVESTIGATION

A. Measurements

The experimental apparatus is shown schematically in Fig. 3. The combustor section consists of a J-47 burner can placed concentrically in a 0.30-m-diameter by 0.77-m-long flow duct. The combustor section is followed by a 0.31-m-diameter by 0.76-m-long spool piece. This section is followed by a 0.30-m-diameter by 6.1-m-long flow duct.

The measurements discussed herein were made at an exit temperature of 920 K and at air mass flow rates of 0.5, 1.13, and 1.68 kg/sec. The corresponding fuel flow rates were 0.009, 0.018, and 0.027 kg/sec. The fuel was similar to JP5. The fuel-air ratio was about 0.02 for this test condition.

Simultaneous internal fluctuating pressure measurements were made at the three locations shown in Fig. 3. The transducers used were conventional 5/8-cm-diameter (nominal) pressure response condenser microphones. To avoid direct exposure to the severe environment within the flow duct, the microphones were mounted outside the duct and the fluctuating pressure in the duct was communicated to the transducers oy "semi-infinite" acoustic waveguides. The internal probes have previously been

used for engine measurements (Refs. 17 to 19) and measurements in a combustion component test facility (Ref. 20). Probe design, frequency response, and operating characteristics are described in Ref. 21.

A typical, constant-bandwidth pressure cross-spectrum phase-angle plot for the frequency range from 2 to 400 Hz is shown in Fig. 4. The test was made with a microphone near the entrance and 5.5 m downstream near the exit of the long duct. The cross-spectrum phase angle data taken at each test condition consisted of 200 data points recorded at 2-Hz intervals.

B. Determination of sound propagation velocity

To obtain the sound propagation velocity, the cross-spectrum phase-angle data are analyzed statistically using the following model. The phase angle θ of the cross spectrum measured between two microphones in the long duct is assumed to be composed of two terms. The first term due to the sound propagation time delay between the two microphones is

$$\theta_1(f) = - \frac{L2\pi f}{c(f) + V} \tag{51}$$

The second term, $\theta_2(f)$, is due to the reflected pressure waves in the duct system. This term is periodic in the frequency domain with a repiod (repetition rate in the frequency domain) given approximately by the round trip travel time between the two microphones:

$$\tau_R = \frac{L}{c(f) + V} + \frac{L}{(f) - V} = \frac{1}{f_R} \tag{52}$$

The following procedure estimates both terms. Thus, the procedure analytically separates this second term from the cross-spectrum phase angle so that the sound propagation velocity can be calculated from an estimate of the first term.

The first step in obtaining the sound propagation velocity is to curve fit the measured phase-angle data. The curve fit is calculated by first using a linear least squares curve fit. Then, a finite Fourier series analysis in the frequency domain is used to fit the remainder. Consequently, the curve fit function is

$$\hat{\Theta}(f) = \bar{\Theta} - \frac{L2\pi f}{\bar{c} + V} + \sum_{j=1}^{N} c_j \cos(j\tau_1 2\pi f) + \sum_{j=1}^{N} b_j \sin(j\tau_1 2\pi f) \qquad (53)$$

where

$$\tau_1 = \frac{1}{f_{max}} \qquad (54)$$

$$c_j = \frac{2}{f_{max}} \int_0^{f_{max}} \Theta(f)\cos(j\tau_1 2\pi f) \, df \qquad (55)$$

and

$$b_j = \frac{2}{f_{max}} \int_0^{f_{max}} \Theta(f)\sin(j\tau_1 2\pi f) \, df \qquad (56)$$

While this function fits exactly, it is not useful unless it fulfills the following requirements: (1) the number of terms is small; (2) the terms can be physically identified; and (3) the resulting curve fit remains valid. Thus, the second step was to study the curve fit with these requirements in mind. From a study of various suboptimal curve fits it was determined that using only the eight or nine terms with the largest coefficients was sufficient to give a standard deviation of approximately 10°. Furthermore, an examination of these terms showed that they fell into two groups. One set of terms corresponded to time constants near τ_R and $2\tau_R$. Consequently, these are assumed to be due to the reflected waves in the duct system. Since the second set corresponds to time constants of τ_1 and $2\tau_1$, they are assumed to be related to $c(f)$. Consequently, the sound propagation speed is evaluated from

$$\hat{\Theta}(f) = -\frac{L2\pi f}{\hat{c}(f) + V} = -\frac{L2\pi f}{\bar{c} + V} + \sum_{j=1}^{2} \left[c_j \cos(j\tau_1 2\pi f) + b_j \sin(j\tau_1 2\pi f) \right] \qquad (57)$$

at high enough frequencies that the Fourier series terms are second order. At low frequencies it is assumed that $\hat{c}(f) = \bar{c}(f)$. The mean flow velocities V calculated using the measured air mass flow rate, the measured

18

temperature, and the duct geometry were 18.5, 41.6, and 61.3 m/sec for the
0.5, 1.13, and 1.68 kg/sec air mass flow rate test conditions, respectively.

The estimated sound propagation velocities calculated using Eq. (57)
are shown in Fig. 5. Figure 5 shows that for all three test conditions the
sound propagation velocity is below the adibatic speed of sound (610 m/sec).
Moreover, for the two lowest velocity test conditions, the sound propaga-
tion velocity is near the isothermal sound propagation speed of 515 m/sec.
The experimental results indicate that the sound propagation speed increases
with the frequency above 200 Hz. Finally, the sound propagation speed dis-
persion relation apparently varies with the test conditions. These experi-
mental results are in good agreement with those predicted by the simple
theory presented herein.

III. COMPARISON OF MEASUREMENT AND THEORY

The measured cross-spectrum phase-angle analysis indicates that the
sound propagation speed is near the isothermal sound propagation speed
and does not vary at low frequencies. This result can easily be related
to the analysis used here and in Ref. 8 if the additional assumptions are
made that soot particle temperature, mass transfer, and viscous drag force
perturbations are small and that $\omega \tau_s / \mathscr{N}_s$ is less than one. With these
assumptions, Eqs. (21) and (3), with the density perturbation eliminated
by substituting the perfect gas perturbation state equation, can be used
to eliminate the bulk gas temperature perturbation and to find a relation
between the bulk gas entropy perturbation and the pressure perturbation.
Using Eq. (7) at low frequencies with these assumptions yields

$$\frac{P(\omega)}{2\rho_o c_o(-i\omega)} + \frac{S(\omega)}{2c_p} + \frac{H(\omega)}{2p_o(-i\omega)} = \frac{1-\gamma}{2} \tag{58}$$

From Eqs. (4) and (54) the propagation wave number is

$$ik_o \Omega = ik_o\left(\frac{1}{2} + \frac{\gamma}{2}\right) \tag{59}$$

and from Eq. (9) the sound propagation velocity is given by

$$c(\omega) = \frac{c_o}{\frac{1}{2} + \frac{\gamma}{2}} \tag{60}$$

Thus, for $\gamma = 1.4$ the sound propagation speed is 0.83 c_o or 506 m/sec. Note that if the wave number equation had not been linearized by replacing $(1 - \beta)^{1/2}$ by $1 - \beta/2$, it would be easy to show that the propagation speed would be given by $c_o/\sqrt{\gamma}$, which is exactly equal to the isothermal speed of sound (515 m/sec).

The same result is obtained if similar assumptions are applied to the theory of plane wave propagation in a liquid fuel droplet cloud. Thus, for these cases sound propagation is isothermal at low frequencies due to heat transfer from the soot particle or liquid fuel droplet. The experimental results indicate that heat transfer from the soot particle or liquid fuel droplet cloud to the bulk gas is the major effect, since the propagation velocity obtained is near the isothermal speed of sound and seems to be constant at low frequencies.

The occurrence of sound propagation at velocities less than the isentropic velocity in combustors has not been reported previously. However, the propagation of sound at the isothermal velocity rather than at the isentropic velocity and the gradual transition from the isothermal conditions at low frequencies to isentropic at high frequencies have been identified previously in sound absorbing materials (Ref. 22). In addition, Dobbins and Temkin studied (Ref. 4) sound propagation in a gas-particle mixture as a factor in solid propellant rocket motor acoustic combustion instability. They noted that the addition of particles can change the characteristic frequency in a fixed geometry combustion system. The proposed interaction between combustor emissions from a liquid fuel combustor and the plane wave propagation is advanced herein as the reason for the previously observed anomalies.

IV. CONCLUSIONS

Dispersion and attenuation of acoustic plane wave disturbances propagating in a ducted combustion system caused by fuel droplet and soot emissions from a jet engine combustor have been studied experimentally and theoretically. The cross-spectrum phase angle measured between two microphones has been used to evaluate the sound propagation speed. The following conclusions were reached:

1. Fuel droplet and soot emissions from jet engine combustors may attenuate and change the plane wave propagation velocity by heat transfer and mass transfer with the ambient gas.

2. Sound propagation tends to be isothermal at low frequencies as predicted.

3. In order to predict the frequency variation of resonance peaks in a combustion noise spectra measured in a duct, the soot and hydrocarbon emissions must be considered and the physics and chemistry of acoustic-emission interaction must be understood.

V. REFERENCES

1. P. S. Epstein and R. R. Carhart, J. Acoust. Soc. Am., 25, 553-565 (1953).

2. J. C. F. Chow, J. Acoust. Soc. Am., 36, 2395-2401 (1964).

3. S. Temkin and R. A. Dobbins, J. Acoust. Soc. Am., 40, 317-324 (1966).

4. R. A. Dobbins and S. Temkin, AIAA J., 5, 2182-2186 (1967).

5. F. E. Marble and D. C. Wooten, The Phys. Fluids, 13, 2657-2664 (1970).

6. G. A. Davison, J. Atmos. Sci., 32, 2201-2205 (1975).

7. J. E. Cole and R. A. Dobbins, J. Atmos. Sci., 28, 202-209 (1971).

8. F. E. Marble and S. M. Candel, AIAA J., 13, 634-639 (1975).

9. "Aircraft Engine Emissions," NASA CP-2021 (1977).

10. G. M. Faeth, "Current Status of Droplet and Liquid Combustion," Paper presented at the Combustion Institute, Spring Technical Meeting, Cleveland, Ohio, March 28-30 (1977).

11. D. Harrje, ed., "Liquid Propellant Rocket Combustion Instability," NASA SP-194 (1972).

12. L. H. Linden and J. B. Heywood, Combust. Sci. Technol., 2, 401-411 (1971).

13. C. T. Norgren, "Determination of Primary-Zone Smoke Concentrations from Spectral Radiance Measurements in Gas Turbine Combustors," NASA TN D-6410 (1971).

14. P. C. Gouldin, Combust. Sci. Technol., 7, 33-45 (1973).

15. F. Wright, "The Oxidation of Soot by O Atoms," International Symposium on Combustion, 15th (Combustion Institute, Pittsburgh, Pa., 1975), pp. 1449-1459.

16. G. A. Simons and P. F. Lewis, "Mass Transport and Heterogeneous Reactions in a Porous Medium," Paper presented at the Combustion Institute, Spring Technical Meeting, Cleveland, Ohio, March 28-30 (1977).

17. M. Reshotko, A. Karchmer, P. F. Penko, and J. G. McArdle, "Core noise measurements on a YF-102 turbofan engine," AIAA Paper 77-21 (Jan. 1977).

18. A. M. Karchmer, M. Reshotko, and F. J. Montegani, "Measurement of far field combustion noise from a turbofan engine using coherence functions," AIAA Paper 77-1277 (Oct. 1977).

19. A. Karchmer and M. Reshotko, "Core noise source diagnostics on a turbo-fan engine using correlation and coherence techniques," NASA TM X-73535 (1976).

20. M. Reshotko and A. Karchmer, "Combustor Fluctuating Pressure Measurements In-engine and in a Component Test Facility -- A Preliminary Comparison," NASA TM-73845 (1977).

21. A. M. Karchmer, "Identification and Measurement of Combustion Noise from a Turbofan Engine Using Correlation and Coherence Techniques," Ph. D. Thesis, Case Western Reserve Univ., Cleveland, Ohio (1978).

22. L. L. Beranek, "Acoustical Properties of Homogeneous, Isotropic Rigid Tiles and Flexible Blankets," J. Acoust. Soc. Am., 19, 556-568 (1947).

TABLE I. - Parameters[a] used to calculate dispersion and attenuation
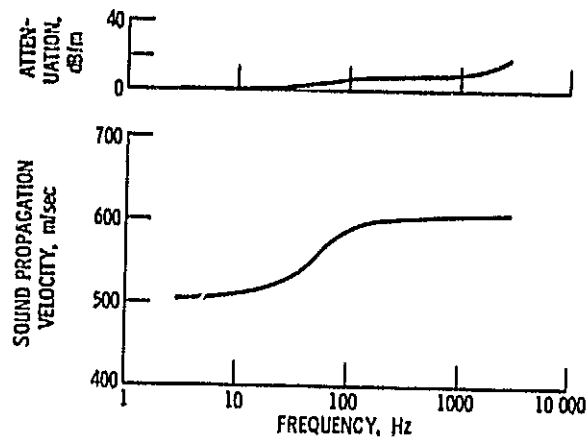
for the case of fuel droplets vaporizing

T, K 922.0	$\mathcal{R}_v$ 0.05
κ, W/m-K . . . . 5.38×100^{-2}	h_{LV}, J/kg . . . . 4.16×10^7
ρ_o, kg/m^3 . . . . 0.378	NM, kg/m^3 . . . . 0.0058
c_p, J/kg-K 1100.0	c_o, m/sec 610.0
γ 1.4	η, $H_{LV}/T_o c_p$ 41
ρ_L, kg/m^3 . . . . 845.0	β, $(MW)_v/(MW)_g$ 3.94
c_L, J/kg-K 1700	N . . . . 1.64×10^{13}
r_L, m . . . . 11.0×10^{-6}	m_L, kg . . . . 3.54×10^{-15}
$(MW)_g$ 28.97	$\mathcal{R}_L$, NM_L/ρ_o . . . . 1.53×10^{-2}
$(MW)_L$ 114.0	τ, sec . . . . 5.13×10^{-6}
μ, kg/m-sec . . . . . . 3.66×10^{-5}	τ_D, sec . . . . 1.64×10^{-5}
D_{vg}, m^2/sec . . . . 4.54×10^{-5}	τ_T, sec . . . . 1.18×10^{-5}

[a]Defined in Ref. 8.

TABLE II. - Parameters used to calculate dispersion and attenuations
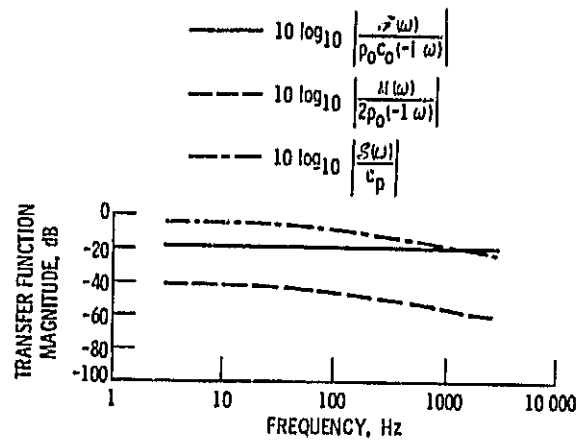
curves for the case of soot particles oxidizing

T, K	922.0	Q, J/kg	-3.637×10^6	
K, W/m-K	5.38×10^{-2}	A_I, m^2/kg	4.0×10^8	
ρ, kg/m^3	0.378	c_o, m/sec	609.0	
c_p, J/kg-K	1100.0	ϵ, $Q/T_o c_p$	-3.585	
γ	1.4	k_a, kg/N-sec	8.08×10^{-10}	
ρ_s, kg/m^3	1880.0	$\zeta \frac{T_o}{k_a} \frac{dK_a}{dT}$	17.0	
c_s, J/kg-m^3	3200.0			
r_s, m	1.0×10^{-6}	m_s, kg	7.87×10^{-15}	
$(MW)_g$	28.97	τ, sec	1.14×10^{-5}	
μ, kg/m-sec	3.66×10^{-5}	τ_T, sec	1.50×10^{-6}	
X_{O_2}	0.05	τ_A, sec	3.09×10^{-5}	

	Example	
	1	2
N	7.36×10^{13}	6.73×10^{12}
Nm_s, kg/m^3	5.8×10^{-3}	5.8×10^{-4}
X_s, Nm_s/ρ_o	1.5×10^{-3}	1.5×10^{-3}

(a) ATTENUATION AND DISPERSION.

Figure 1. - Fuel droplets vaporizing.

$$10 \log_{10} \left| \frac{\vec{z}(\omega)}{\rho_0 c_0 (-i\,\omega)} \right|$$

$$10 \log_{10} \left| \frac{u(\omega)}{2\rho_0 (-i\,\omega)} \right|$$

$$10 \log_{10} \left| \frac{s(\omega)}{c_p} \right|$$
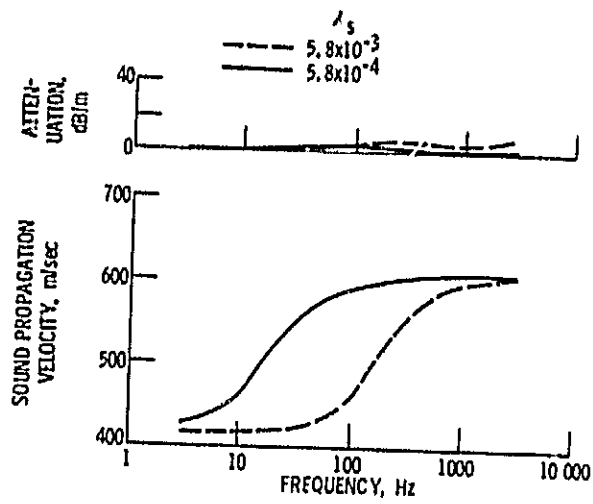
(b) TRANSFER FUNCTIONS.

Figure 1. - Concluded.

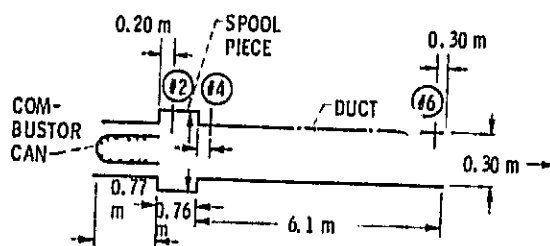Figure 2. - Attenuation and dispersion for oxidizing soot particles.
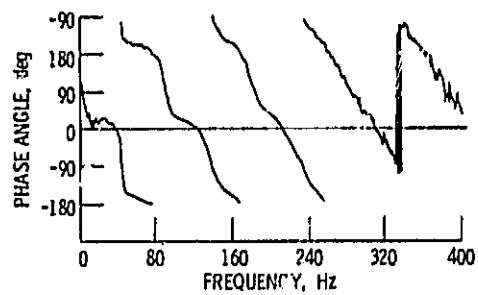

Figure 3. - Ducted combustion system.

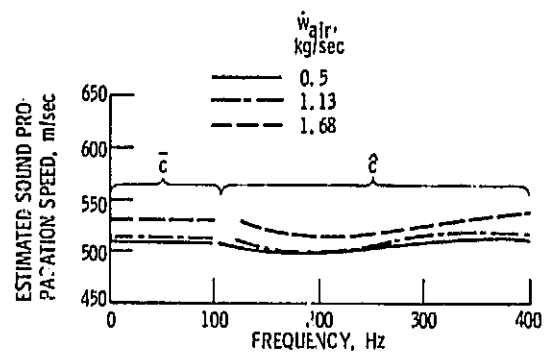Figure 4. - Cross-spectrum phase angle between long flow duct entrance and exit pressure perturbation. ($\dot{W}_{air}$ = 0.5 kg/sec).

Figure 5. - Estimated sound propagation speed.